

Determining hydrodynamic boundary conditions from equilibrium fluctuationsShuyu Chen,¹ Han Wang,^{2,3} Tiezheng Qian,⁴ and Ping Sheng^{1,5,*}¹*Department of Physics, Hong Kong University of Science and Technology, Clear Water Bay, Kowloon, Hong Kong, China*²*CAEP Software Center for High Performance Numerical Simulation, Beijing, China*³*Zuse Institute Berlin, Takustrasse 7, 14195 Berlin, Germany*⁴*Department of Mathematics, Hong Kong University of Science and Technology, Clear Water Bay, Kowloon, Hong Kong, China*⁵*Institute for Advanced Study, Hong Kong University of Science and Technology, Clear Water Bay, Kowloon, Hong Kong, China*

(Received 24 November 2014; revised manuscript received 4 September 2015; published 7 October 2015)

The lack of a first-principles derivation has made the hydrodynamic boundary condition a classical issue for the past century. The fact that the fluid can have interfacial structures adds additional complications and ambiguities to the problem. Here we report the use of molecular dynamics to identify from equilibrium thermal fluctuations the hydrodynamic modes in a fluid confined by solid walls, thereby extending the application of the fluctuation-dissipation theorem to yield not only the accurate location of the hydrodynamic boundary at the molecular scale, but also the relevant parameter value(s) for the description of the macroscopic boundary condition. We present molecular dynamics results on two examples to illustrate the application of this approach—one on the hydrophilic case and one on the hydrophobic case. It is shown that the use of the orthogonality condition of the modes can uniquely locate the hydrodynamic boundary to be inside the fluid in both cases, separated from the molecular solid-liquid interface by a small distance Δ that is a few molecules in size. The eigenvalue equation of the hydrodynamic modes directly yields the slip length, which is about equal to Δ in the hydrophilic case but is larger than Δ in the hydrophobic case. From the decay time we also obtain the bulk viscosity which is in good agreement with the value obtained from dynamic simulations. To complete the picture, we derive the Green-Kubo relation for a finite fluid system and show that the boundary fluctuations decouple from the bulk only in the infinite-fluid-channel limit; and in that limit we recover the interfacial fluctuation-dissipation theorem first presented by Bocquet and Barrat. The coupling between the bulk and the boundary fluctuations provides both the justification and the reason for the effectiveness of the present approach, which promises broad utility for probing the hydrodynamic boundary conditions relevant to structured or elastic interfaces, as well as two-phase immiscible flows.

DOI: [10.1103/PhysRevE.92.043007](https://doi.org/10.1103/PhysRevE.92.043007)

PACS number(s): 47.61.–k, 47.11.–j, 68.08.–p, 83.50.Lh

I. INTRODUCTION

In contrast to the electromagnetic Maxwell equations in which the boundary conditions can be derived from the equations themselves, the hydrodynamic boundary condition represents information that is additional to the Navier-Stokes equation, and necessary for its solution. It is a classical issue dating back to the work of Maxwell on the kinetic theory of gases [1,2]. Over the years, there have been many studies addressing this problem from the perspectives of kinetic theory [3–7], fluctuations [8–21], and the Onsager principle [22–24]. At the molecular level, the hydrodynamic boundary condition is complicated by the fluid structure near the solid boundary [9,13,25–29], which introduces an ambiguity to the location at which the hydrodynamic boundary condition should be applied. Approaches involving dynamic experiments [30–33] or simulations [9–29] for determining the hydrodynamic boundary condition and its relevant parameters usually suffer from complications, such as the precise location of the hydrodynamic boundary, as well as effects inherent to dynamics that make the hydrodynamic boundary condition imprecise at the molecular scale. The fluctuation-dissipation theorem (FDT) [34], a remarkable relation linking the macroscopic linear response coefficients to the microscopic correlation functions, represents an obvious avenue to obtain the parameters of the

hydrodynamic boundary condition from molecular dynamics (MD) simulations. Bocquet and Barrat [9] pioneered in writing down the relevant FDT for the fluid-solid interfacial dissipation coefficient for a semi-infinite fluid bounded by a solid boundary. However, subsequent adaptation of its use in molecular dynamics simulations of finite fluid systems has yielded results that are sample-size dependent [12,13,21]. In particular, Petracic and Harrowell performed a series of works showing that the friction coefficient obtained by applying Bocquet-Barrat theory corresponds to an empirical friction coefficient with clear geometric dependence on the channel width, rather than the intrinsic friction coefficient that should be solely determined by the interfacial characteristics [10,12,13]. In particular, it was shown that the force autocorrelation integral calculated from MD simulations varies inversely with the sum of the channel width plus twice the slip length. This behavior is in contradiction to the expectation of a constant value that would correspond to the intrinsic interfacial friction coefficient as proposed by Bocquet and Barrat. Similar observations and objections have been reported by others [16,18,21], supported by numerical evidence. Since the intrinsic interfacial friction arises physically from the presence of a liquid-solid interface, information regarding the interfacial friction should be fully describable for a nanoconfined system where the number of liquid molecules is finite and far from the thermodynamic limit. Hence the attribution of such size-dependent effect to the intrinsic limitation of a finite system is clearly untenable [21]. There were also reports that the application of

*Corresponding author: sheng@ust.hk

Bocquet-Barrat theory leads to an interfacial friction coefficient that is inconsistent with that obtained from nonequilibrium MD simulations [13,21]. A related issue is that the derivation of the Bocquet-Barrat theory assumed only the mode with eigenvalue $k_0 = 0$ [9] to be relevant to the hydrodynamic boundary condition, where k_n denotes the periodicity of the n th hydrodynamic mode along the (fluid) channel width direction. However, in any simulations of finite, confined systems, the removal of the center-of-mass motion, e.g., by considering only antisymmetric modes, would imply that $k_0 = 0$ is a trivial solution to the eigenvalue equation that possesses no thermal energy. This fact is clearly demonstrated below in our simulation results, and has the implication that for finite, confined systems, only those finite-energy modes with $k_n \neq 0$ (which also satisfy the eigenvalue equation for the hydrodynamic modes) should be considered as the source of information for the hydrodynamic boundary condition that is derivable from the fluctuation-dissipation theorem. In fact, in the last section of this work we derive a fluctuation-dissipation theorem for a confined system, and show that the theory of Bocquet and Barrat can be recovered in the infinite-channel-width limit. Hence, in spite of all the criticisms in the previous literature, the theory of Bocquet and Barrat is actually correct; it is just inapplicable to finite systems and consequently cannot be useful for obtaining the hydrodynamic boundary condition information through MD simulations.

Apart from the issues raised by the theory of Bocquet and Barrat, a serious problem for obtaining the intrinsic hydrodynamic interfacial friction coefficient through MD simulations is the lack of completeness and consistency in determining all the hydrodynamics parameters [9,13,14,16,21,29]. In particular, the precise microscopic position of the hydrodynamic boundary is a persistent problem that seems to lie beyond any consistent framework. Owing to the liquid structures near the solid boundary, an arbitrariness is usually introduced in determining the reference surface at which the slip velocity should be measured. Consequently, there can be an uncertainty in the value of the slip length and the relevant friction coefficient [13,14,21]. Similar arbitrariness can also arise for those methods in which a boundary “slab” is introduced and the boundary properties are measured inside this artificial region [16]. Denniston and Robbins [29] have reported that a major difficulty in finding the hydrodynamic boundary condition arises from the necessary arbitrariness in determining the position of the hydrodynamic boundary from MD simulation results, owing to the fact that the system is always underdetermined within the traditional frameworks. Even the sharpness of the hydrodynamic boundary, which has been an implicit classical assumption, has so far not been explicitly tested. If it turns out that the hydrodynamic boundary is not sharp in the microscopic scale, then the concept of a slip length would become meaningless since such a length must be measured from a sharp reference surface. This is especially the case if the slip length is on the order of the molecular scale, as is generally the case.

In this work, we take the approach of using MD simulation data to answer all those questions and problems raised above, with no *a priori* assumptions. It is shown that in a confined fluid system, as equipartition of thermal energy dictates the excitation of hydrodynamic eigenmodes with equal kinetic

energy, these eigenmodes can be unambiguously identified in molecular dynamics simulations through the projection approach. By using the wave numbers k_n of the hydrodynamic modes as well as the mutual orthogonality of the eigenfunctions, the multiple eigenmodes form an overdetermined system for the unique determination of the precise location of the hydrodynamic boundary, the interfacial dissipation coefficient, and the viscosity. In other words, we use the MD simulation data to test the classical assumption of a sharp hydrodynamic boundary. We find overwhelming consistency, even for the large k_n modes, provided that the fluid motion at the microscopic level is long-time averaged. Such consistency is manifested by the fact that multiple pairs of the hydrodynamic modes, identified through the MD data projection approach, can simultaneously satisfy the orthogonality condition over the *same spatial domain*. This is possible only if the hydrodynamic boundary is sharp and uniquely defined. Indeed, the position of the hydrodynamic boundary thus defined is found to be inside the fluid domain, separated from the fluid-solid molecular interface by a small distance. Since in a confined system the hydrodynamic modes inherently contain the information about the hydrodynamic boundary condition, this approach enables us to obtain unambiguous information about the slip length. A side benefit is that the bulk viscosity can also be deduced and is shown to be in good agreement with the value obtained from bulk simulations.

In what follows, Sec. II presents a description of the hydrodynamic modes in the continuum limit. Our scheme is delineated in Sec. III, and denoted the generalized fluctuation-dissipation approach. Details about the molecular dynamics simulations are given in Sec. IV, followed by the presentation and discussion of results for two cases—one hydrophilic and one hydrophobic—in Sec. V. Section VI presents the derivation of the Green-Kubo relation [35,36] for a confined system, which provides not only the theoretical (fluctuation-dissipation) context for our approach, but also the limiting scenario under which the theory of Bocquet and Barrat is recovered.

II. HYDRODYNAMIC MODES

Consider a system of incompressible fluid confined between two parallel planar solid walls with a separation of $2H$, shown schematically in Fig. 1. The z coordinate is defined to be

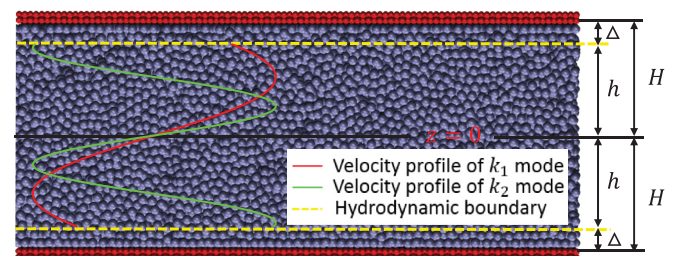


FIG. 1. (Color online) Geometry of the system and the hydrodynamic modes. Molecular view of a sample simulation system showing the definition of H , h , and Δ . Two hydrodynamic modes are also shown. They correspond to the hydrophilic case with $H = 13.2\sigma$, where σ is the size parameter in the Lennard-Jones potential.

normal to the solid walls, with $z = 0$ at the center of the fluid channel. The problem considered is two dimensional, i.e., infinite along the y direction, and the fluid velocity is along the x direction. In thermal equilibrium, the fluctuating transverse (x) momentum density is defined as $J(z,t) = \rho_0 v(z,t)$, where ρ_0 is the density of the fluid and $v(z,t)$ is the fluctuating transverse velocity. $J(z,t)$ may be expanded as $J(z,t) = \sum_{n=1}^{\infty} j_n(z,t)$, with the eigencomponents $j_n(z,t)$ obtainable by solving the incompressible Navier-Stokes equation, which can be reduced in the present case to the following simple form:

$$\frac{\partial}{\partial t} j_n(z,t) = \frac{\eta}{\rho_0} \frac{\partial^2}{\partial z^2} j_n(z,t). \quad (1)$$

Equation (1) may be solved through separation of variables. Using $j_n(z,t) = Z_n(z)T_n(t)$, we have

$$\frac{1}{Z_n(z)} \frac{d^2 Z_n(z)}{dz^2} + k_n^2 = 0 \quad (2a)$$

and

$$\frac{\rho_0}{\eta T_n(t)} \frac{dT_n(t)}{dt} + k_n^2 = 0. \quad (2b)$$

Note that only the antisymmetric fluctuating modes are considered in the present study, as the center-of-mass motion is removed from the problem. It follows that $Z_n(z) = A_n \sin(k_n z)$ and $T_n(\Delta t) = T_n(0) e^{-\eta k_n^2 \Delta t / \rho_0}$, where Δt denotes the time relative to an arbitrary starting point. The coefficient A_n and the wave number k_n can be determined from the initial condition of equipartition and the Navier boundary condition (NBC), respectively. For the k_n mode, the slip velocity v_n^{slip} is defined as the fluid velocity at the hydrodynamic boundary $z = \pm h$, where $h \leq H$, with regard to the corresponding velocity pattern $z_n(z) = Z_n(z)/\rho_0$. That is:

$$\rho_0 v_n^{\text{slip}} = A_n \sin(k_n h). \quad (3a)$$

Moreover, the force balance in the boundary layer means that the frictional stress exerted by the wall on the slipping fluid, $G_n^{\text{fric}} = -\beta v_n^{\text{slip}}$, must be fully accounted for by the tangential viscous stress at the hydrodynamic boundary, $G_n^{\text{visc}} = \eta \frac{\partial z_n(z)}{\partial z} |_{z=h}$, for each mode, yielding the equation

$$-\beta \rho_0 v_n^{\text{slip}} = \eta A_n k_n \cos(k_n h). \quad (3b)$$

Here β is the slip frictional coefficient and η is the viscosity of the fluid. Dividing Eq. (3a) by Eq. (3b) and introducing the slip length $l_{\text{slip}} = \eta/\beta$, we get the equation

$$\tan(k_n h) = -k_n l_{\text{slip}} \quad (4)$$

for all the eigenmodes. It is important to note here that the hydrodynamic boundary $z = \pm h$ can differ from the fluid-solid molecular interface $z = \pm H$. Owing to the orthogonality of the eigenmodes (as they constitute the eigenfunctions of a real symmetric operator), h should be uniquely defined as the domain over which the inner product of $j_m(z,t)$ and $j_n(z,t)$ is zero if $m \neq n$ [the orthogonality condition ensured by Eq. (4)]. Furthermore, due to the antisymmetric nature of the modes, it is necessary to only consider half the system. We also note that for a finite fluid system the $k_0 = 0$ mode does not have any kinetic energy and therefore represents the trivial solution of the eigenvalue equation.

III. A GENERALIZED FLUCTUATION-DISSIPATION APPROACH

By utilizing the hydrodynamic modes and the equipartition theorem, one can write down the FDT for the whole system. This is shown in the last section so as not to digress from our main line of presentation. What is important to note is that the boundary fluctuations are intimately coupled with the bulk fluctuations, and the two would decouple only in the limit of $H \rightarrow \infty$, in which case we recover the interfacial FDT as first formulated by Bocquet and Barrat [9]. Below we propose a different approach which may be regarded as a generalization of the FDT to this finite system.

All the eigenmodes satisfy Eq. (4), which ensures mutual orthogonality. If a few low lying eigenmodes can be identified with k_n being accurately measured, then both h and l_{slip} can be determined. We start by measuring the normalized transverse momentum density autocorrelation function $C(k, \Delta t)$ from molecular dynamics simulations. Here k is taken to be a continuous variable. Owing to the linear response theory [37] and the exponential form of $T_n(\Delta t)$, it may be concluded that $C(k_n, \Delta t) = T_n(\Delta t)/T_n(0) = \exp(-\eta k_n^2 \Delta t / \rho_0)$, with a decay time $\tau_{\text{decay}}(k_n) = \rho_0 / \eta k_n^2$. Since the independent hydrodynamic modes are preferably excited, their decay times should be manifest as (local) peaks in the corresponding k spectrum. This can also be demonstrated by solving Eq. (1) as an initial value problem with $j_n(z, t = 0) = \sin k z$ as the initial pattern, where k can take any value. Deviation of the k value from k_n would introduce inconsistency with the boundary condition, thereby leading to a faster decay of the initial pattern.

From the above, a straightforward method suggests itself for identifying the k_n modes in a confined fluid system by MD simulations. That is, we let the fluid system, through its fluctuations, tell us directly about the information contained in the hydrodynamic modes. From the peak decay times one can uniquely determine the viscosity η of the confined fluid (as the density of the fluid is generally well defined). From the k_n positions one can identify the location of the hydrodynamic boundary $z = h$ by applying the condition $\int_0^h \sin(k_n z) \sin(k_m z) dz = 0$ for any pair $n \neq m$. For different pairs, the h values thus obtained can be checked for consistency. Provided the h values display only very small discrepancies for the different pairs of $n \neq m$, Eq. (4) can then be numerically solved by adjusting the only unknown parameter l_{slip} . Dividing η by l_{slip} then yields the value of the slip frictional coefficient β . By carrying out this approach for different channel widths, one can check the expectation that the parameters $\Delta = H - h$ and β should be independent of the channel width, as they pertain only to the fluid-solid interface. If it happens that we find any inconsistency between the hydrodynamic description and the MD simulation results, then our approach will be able to tell us the deviation between the hydrodynamic description and the actual fluid system behavior at the molecular scale. Such information can be valuable in formulating corrections to the hydrodynamic theory at the nanoscale. In this work, the results are shown to give overwhelming support to the hydrodynamic description, even at the molecular scale.

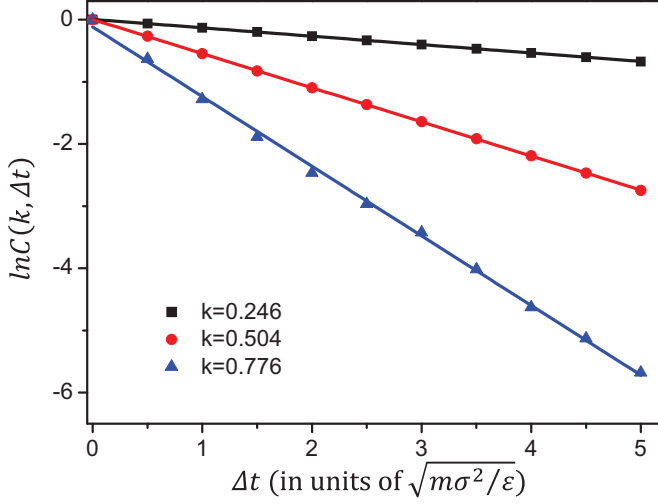


FIG. 2. (Color online) Decay of the hydrodynamic modes. Natural logarithm of the normalized autocorrelation functions measured from MD simulations for the three eigenmodes in the hydrophilic channel with $H_1 = 13.2\sigma$. The decay time can be evaluated from the inverse of the slope for each straight line.

IV. MOLECULAR DYNAMICS SIMULATIONS

MD simulations of a Lennard-Jones (LJ) fluid, confined between two parallel planar solid walls, were performed to demonstrate the implementation of our method. The wall atoms were arranged in a face-centered-cubic lattice and constrained to be in the vicinity of the lattice sites by a harmonic spring potential. The force constant was chosen to ensure that the mean square displacement of wall atoms does not exceed 10% of the nearest-neighbor distance, obeying the Lindemann criterion [22]. Interactions between the wall atoms were removed. Each wall comprised two [001] atomic planes perpendicular to the z axis [22–24,27,38]. Periodic boundary conditions were imposed along the x and y directions. We have carried out simulations on three systems with the equilibrium positions of the two interfacial [001] wall planes at $z = \pm H_1 = \pm 13.2\sigma$, $z = \pm H_2 = \pm 26.1\sigma$, and

$z = \pm H_3 = \pm 51.9\sigma$. Here σ is the LJ potential’s molecular size parameter (see below). In addition, for each channel width we considered both a hydrophilic scenario and a hydrophobic scenario, by varying the attractive term in the LJ potential for fluid-wall interaction [13,22,26] while keeping the atomic configuration of the walls, the fluid density, and the fluid-fluid interaction unchanged. Both the fluid-fluid and wall-fluid atomic interactions are described by the LJ potentials $u_{ij}(r) = 4\epsilon_{ij}[(\sigma_{ij}/r)^{12} - \delta_{ij}(\sigma_{ij}/r)^6]$, where i and j can be either “ f ” for fluid or “ w ” for wall. In the present study, the reduced LJ-unit system was adopted, with $\epsilon_{ff} = \epsilon$, $\epsilon_{wf} = 1.16\epsilon$, $\sigma_{ff} = \sigma$, $\sigma_{wf} = 1.04\sigma$, and $\delta_{ff} = 1$. For the hydrophilic scenario, we set $\delta_{wf1} = 1$, whereas for the hydrophobic scenario we set $\delta_{wf2} = 0.7$. Here the terms “hydrophilic” and “hydrophobic” are used to distinguish the slightly different degrees of wettability of the two cases. The fluid is wetting to the wall (with a contact angle smaller than 90°) in both cases [13]. It should be noted that the equilibrium wall-fluid atomic distance for the hydrophobic scenario has been estimated to be only $\sim 0.1\sigma$ larger than that for the hydrophilic scenario [13], much smaller than the channel width.

The main purpose of considering both hydrophobic and hydrophilic scenarios is to demonstrate that the consistency and validity of our approach hold for different cases of wall-fluid interaction. All the LJ interactions are cut off at $r_c = 2.5\sigma$. The additional noise introduced by the cutoff has been noted to be negligible, with the total energy remaining constant and the kinetic energy oscillating around the equilibrium value [38,39]. The atomic mass is denoted by m , and the average number density for the fluid is set at $\rho_f = \rho_0 = 0.81/\sigma^3$. For wall atoms, the mass is the same as that of the fluid atoms, but the number density is higher, set at $\rho_w = 1.86/\sigma^3$. A constant temperature of $2.8\epsilon/k_B$ was maintained for the two walls using a Langevin thermostat. Throughout the simulations, the equation of motion was integrated with a time step of $0.002\sqrt{m\sigma^2/\epsilon}$. Center of mass motion was removed from the simulation.

From the MD trajectories, the fluctuating transverse momentum density autocorrelation function $C(k, \Delta t)$ was measured for different input values of k ranging from 0.001 to 1 in intervals of 0.001 (all in units of σ^{-1}):

$$C(k, \Delta t) = \frac{\left\langle \left(\sum_{i=1}^N v_i(t=t_0) \sin[kz_i(t=t_0)] \right) \left(\sum_{i=1}^N v_i(t=t_0 + \Delta t) \sin[kz_i(t=t_0 + \Delta t)] \right) \right\rangle}{\left\langle \left(\sum_{i=1}^N v_i(t=t_0) \sin[kz_i(t=t_0)] \right) \left(\sum_{i=1}^N v_i(t=t_0) \sin[kz_i(t=t_0)] \right) \right\rangle}, \quad (5)$$

where $v_i(t)$ and $z_i(t)$ denote the velocity and z coordinate for atom i at time t , respectively. The summation runs over all fluid atoms, and $\langle \rangle$ represents the time averaging. The time resolution of $0.5\sqrt{m\sigma^2/\epsilon}$ was chosen to be two orders of magnitude larger than the simulation time step to ensure that $C(k, \Delta t)$ was measured in the overdamped regime where hydrodynamics should be valid. Here m is the molecular mass and ϵ is the LJ interaction energy unit.

Equation (5) is the expression of the projection approach in which the random thermal velocities are projected onto a k mode so that its normalized time correlation can be evaluated. The decay time $\tau_{\text{decay}}(k)$ was estimated by taking the negative reciprocal of the slope of $\ln[C(k, \Delta t)]$ (plotted as a function of Δt). The exponential decay for the three hydrodynamic modes of the $H_1 = 13.2\sigma$ hydrophilic case are shown in Fig. 2. It is seen that the exponential decay is an extremely accurate description of the data.

V. RESULTS AND DISCUSSION

A. The hydrophilic case

Figure 3 shows the decay time τ_{decay} plotted as a function of k for the three hydrophilic cases. The positions of the peaks corresponding to the eigenmodes k_n were determined by using ORIGIN to subtract the bottom and then locating the peaks. This operation is shown in the inset to Fig. 3(a) for the narrow-channel case of $H_1 = 13.2\sigma$. The results are marked by the red arrows and also tabulated in Table I. It is noted that values of larger k_n 's obtained from MD simulations are not simple multiple integers of the smallest k_1 , owing to the slip boundary condition. The latter is noted to be incorporated in Eq. (4). The viscosity η of the confined fluid can readily be obtained by fitting $\tau_{\text{decay}}(k_n)$ with $\tau_{\text{decay}}(k_n) = \rho_0/\eta k_n^2$, with $\rho_0 = 0.81m/\sigma^3$. The fitting curves (dash-dotted lines) are plotted in Fig. 3 for all three cases. Excellent agreement with the height variation of the eigenmodes is seen. It implies that fluid viscosity is a bulk property and therefore is a manifestation of the fluid-fluid atomic interaction only, regardless of the wall-fluid atomic interactions at the wall-fluid interface. From different cases, all values of η are around $1.84\sqrt{\varepsilon m}/\sigma^2$, consistent with each other and only slightly different from that evaluated by nonequilibrium MD (NEMD) simulations, which are known to display shear-rate dependence [40]. To verify this fact, an average value of $1.88\sqrt{\varepsilon m}/\sigma^2$ for the viscosity is obtained from ten NEMD simulations with different shear rates, with the maximum and minimum at $1.98\sqrt{\varepsilon m}/\sigma^2$ and $1.76\sqrt{\varepsilon m}/\sigma^2$, respectively.

The mutual orthogonality of the eigenmodes can be used to unambiguously determine h so as to locate the hydrodynamic boundary. Then Eq. (4) can be used to determine l_{slip} . We wish to first call attention to the values of k_n tabulated in Table I. For the h (Δ) and l_{slip} values given in each channel width H , remarkable agreement is achieved between all the k_n values measured from MD simulations and those predicted from the hydrodynamic theory. The values of h (Δ) in each case display only very small error bars, obtained by carrying out the orthogonality integration between pairs of modes k_n and k_m , with $n \neq m$. It is seen that in general, the hydrodynamic boundary is located somewhere inside the fluid, with $H > h$ in all the cases. The distance between the molecular solid-liquid interface and the hydrodynamic boundary, $\Delta = H - h$, is dependent on the wall-fluid atomic interaction. However, changing the geometry of the systems does not affect Δ . Hence $\Delta \cong 2.2\sigma - 2.3\sigma$ is an intrinsic parameter of the interface; it is physically associated with the fluid density oscillation near the solid wall, caused by the fluid hydration effect [9,13,25–29].

The slip length l_{slip} , or equivalently the slip frictional coefficient β , is determined by numerically solving Eq. (4) with l_{slip} treated as the only unknown parameter. The resulting solution set $k'_n(h, l_{\text{slip}})$ can be compared with the k_n values obtained from direct MD measurement. The optimal value for l_{slip} that gives the best agreement is shown in Table I. Similarly to the parameter Δ discussed above, l_{slip} is also an intrinsic parameter that depends only on the physical and/or chemical properties of the specific interface, regardless of the system geometry. In the hydrophilic case, l_{slip} is about $2\sigma - 2.1\sigma$ for the present case. Dividing η by l_{slip} gives the value of the slip frictional coefficient $\beta = 0.86 - 0.92\sqrt{\varepsilon m}/\sigma^3$.

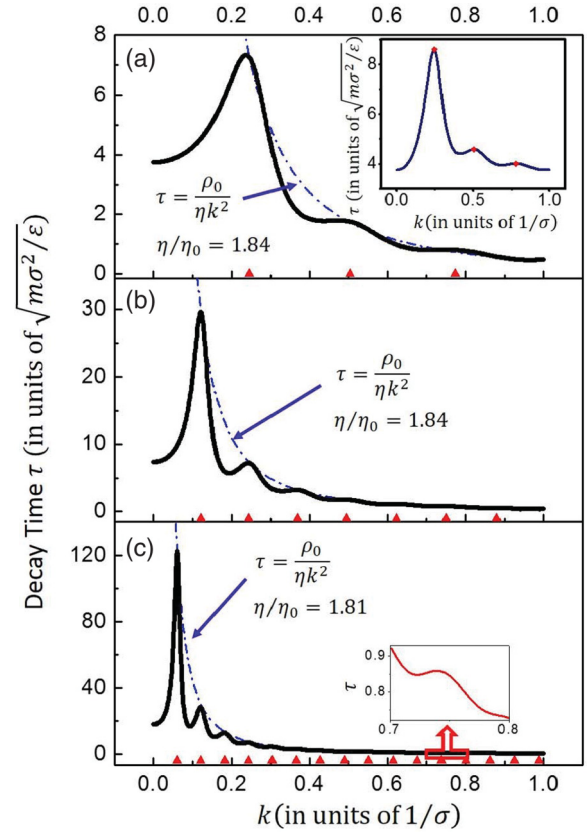


FIG. 3. (Color online) Decay time of the hydrodynamic mode as a function of its wave vector for the hydrophilic channels. (a) For channel width $H_1 = 13.2\sigma$, there are three discernible modes, signified by peaks in the decay time. Their k values are indicated by the red triangles on the horizontal axis. From the orthogonality requirement of the eigenfunctions, these k 's uniquely determine a value of $h = 10.9\sigma$, or $\Delta = 2.3\sigma$ (see Table I). The inset shows the same curve after ORIGIN has subtracted its bottom so as to accurately locate the peak positions (shown as red dots). The dash-dotted curve shows the theoretically predicted decay time of the hydrodynamic mode plotted as a function of k , treated here as a continuous variable. Here ρ_0 denotes the mass density used in the simulations. It is seen that the curve describes extremely well the height variation of the peaks, with $\eta = 1.84\eta_0$ being the value obtained from a best fit to the peak heights. Here $\eta_0 = \sqrt{\varepsilon m}/\sigma^2$ denotes the viscosity unit. This compares favorably with $\eta = 1.95\eta_0$ obtained from bulk simulations. (b) As (a), for $H_2 = 26.1\sigma$. Seven modes can be identified (see Table I), with their k positions indicated by the red triangles. These k 's uniquely determine a value for $h = 23.8\sigma$, or $\Delta = 2.3\sigma$. It should be noted that the value of Δ is almost exactly the same as that in (a), thereby indicating its interfacial characteristic, i.e., independence from H . The dash-dotted curve now corresponds to an η value of $1.84\eta_0$. Again, very good agreement is obtained with the predictions based on hydrodynamic mode description. (c) As (a) and (b), but with $H_3 = 51.9\sigma$. The number of discernible modes has now increased to 16 (see Table I), as indicated by the red triangles. Their agreement with the theory prediction is within 1%. Here $\Delta = 2.2\sigma$. The slipping lengths obtained from the three cases are 2.0 , 2.0 , and 2.1σ for (a), (b), and (c), respectively. It is noted that, for the present hydrophilic case, l_{slip} is approximately equal to Δ . This coincidence makes the nonslip boundary condition, with the boundary set at the molecular interface, very accurate for most of the calculations.

TABLE I. Parameter values for the hydrophilic case.

		$(k_n \text{ in units of } 1/\sigma)$						
		$H = 13.2\sigma, h = 10.9 \pm 0.1\sigma, \Delta = 2.3 \pm 0.1\sigma, l_{\text{slip}} = 2.0 \pm 0.1\sigma, \eta = 1.84\eta_0$						
k_n MD	0.246			0.504				0.777
k_n Theory	0.246			0.504				0.774
		$H = 26.1\sigma, h = 23.8 \pm 0.2\sigma, \Delta = 2.3 \pm 0.2\sigma, l_{\text{slip}} = 2.0 \pm 0.1\sigma, \eta = 1.84\eta_0$						
k_n MD	0.122	0.246	0.371	0.496	0.627	0.756		0.878
k_n Theory	0.122	0.245	0.369	0.495	0.622	0.75		0.879
		$H = 51.9\sigma, h = 49.7 \pm 0.1\sigma, \Delta = 2.2 \pm 0.1\sigma, l_{\text{slip}} = 2.1 \pm 0.1\sigma, \eta = 1.81\eta_0$						
k_n MD	0.061	0.121	0.182	0.244	0.304	0.367	0.428	0.489
k_n Theory	0.061	0.121	0.182	0.243	0.305	0.366	0.428	0.490
k_n MD	0.555	0.611	0.678	0.744	0.795	0.864	0.934	0.98
k_n Theory	0.552	0.614	0.676	0.739	0.801	0.4	0.926	0.989

The MD simulation data can also be employed to test the classical assumption of a sharp hydrodynamic boundary in nanoconfined systems. One piece of evidence is that multiple pairs of the hydrodynamic modes, identified through the MD data projection approach, can simultaneously satisfy the orthogonality condition over the same spatial domain. In addition, the same value of the slip length is obtained for all the hydrodynamic modes at the uniquely defined, sharp hydrodynamic boundary. To demonstrate this, we plot in Fig. 4 the absolute value of $\tan^{-1}\left(\frac{-z_n(z)/z_n'(z)}{l_{\text{slip}}}\right)$ with the k_n values measured from MD simulations for each mode of the hydrophilic case with $H_2 = 26.1\sigma$. Here $z_n(z)$ is the velocity profile for the mode k_n . For each mode, $-z_n(z)/[\partial z_n(z)/\partial z]$ gives exactly the slip length l_{slip} at the hydrodynamic boundary $z = h$. Therefore, we can apply the \tan^{-1} operation to transform the normalized quantity $[-z_n(z)/z_n'(z)]/l_S$ to an angle that equals $\pi/4$ at the hydrodynamic boundary. It can be seen that all the curves intersect at a single point $(h, \pi/4)$. This provides clear evidence that the multiple eigenmodes form an overdetermined system for the unique determination of the precise location of the hydrodynamic boundary and the slip length.

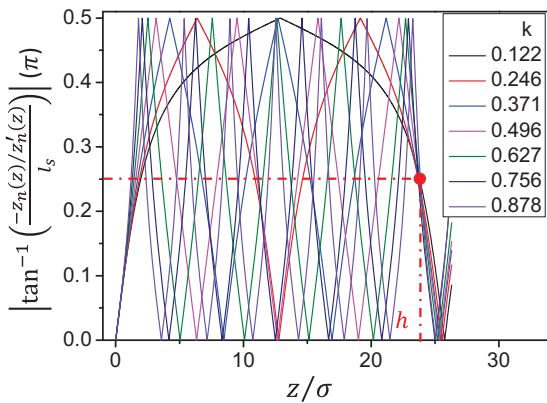


FIG. 4. (Color online) Absolute value of $\tan^{-1}\{[-z_n(z)/z_n'(z)]/l_S\}$ with the k_n measured from MD simulations for each mode of the hydrophilic case with $H_2 = 26.1\sigma$. Here $z_n(z)$ is the velocity profile for mode k_n . The multiple eigenmodes are seen to form an overdetermined system for the unique determination of h , Δ , and l_{slip} .

A direct comparison has been made between the velocity profile obtained from the NEMD simulation of the Poiseuille flow in a hydrophilic channel with $H = 6.7725\sigma$ and that predicted by the hydrodynamic boundary parameter values of our theory. The Poiseuille flow was induced by applying a body force $f = 0.005\epsilon/\sigma$ to each fluid atom along the x direction. As shown in Fig. 5, very good agreement has been achieved. Note that the value of H was purposely chosen to be just half that of the smallest one in the present study (since the deviation from the classical theory prediction is usually the largest for small nanochannels), to demonstrate the applicability of our theory to nanochannel systems.

B. The hydrophobic case

In the hydrophobic case, the less attractive LJ wall-fluid interaction gives rise to a larger contact angle, which, however, is still smaller than 90° [13]. The values of decay time obtained from MD simulations are plotted as a function of k in Fig. 6.

It is to be noted that the value of the viscosity remains about the same as in the hydrophilic case, since it depends

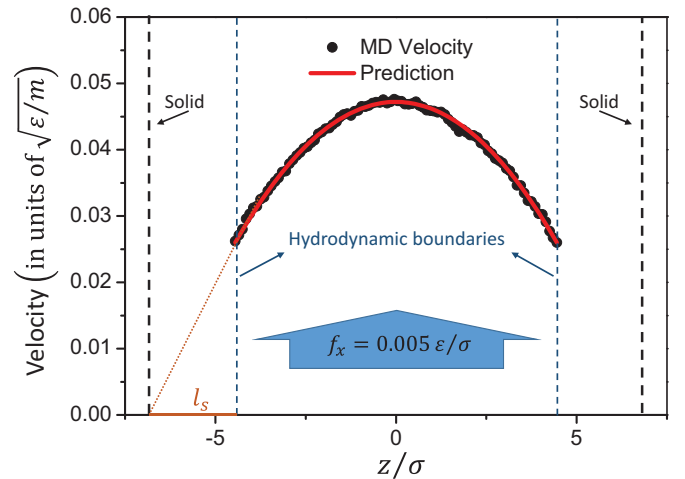


FIG. 5. (Color online) Velocity profile obtained from the NEMD simulation of Poiseuille flow in a hydrophilic channel with $H = 6.7725\sigma$, compared to that predicted by using the hydrodynamic boundary parameter values obtained from our theory. Excellent agreement is seen.

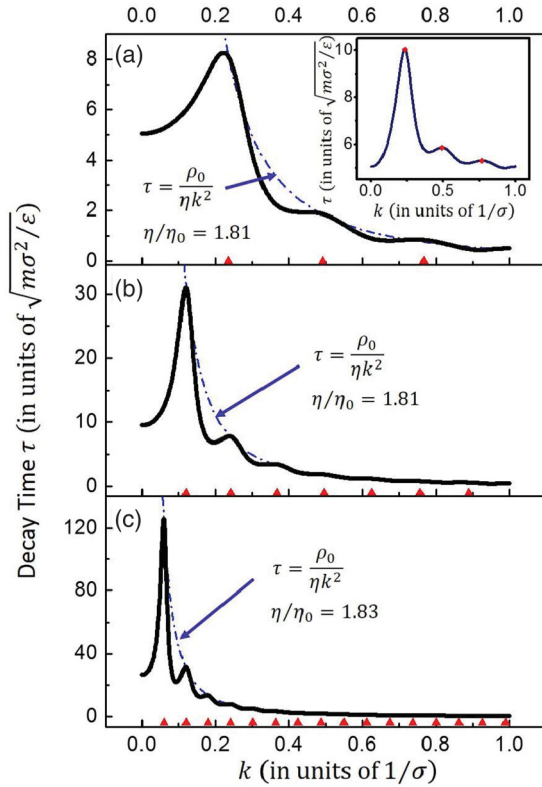


FIG. 6. (Color online) Decay time of the hydrodynamic mode as a function of its wavevector for the hydrophobic channels. (a) For channel width $H = 13.2\sigma$, there are three discernible modes, with their k values indicated by the red triangles. These k 's uniquely determine a value for $h = 10.8\sigma$ or $\Delta = 2.4\sigma$ (see Table II). The inset shows the same curve after ORIGIN has subtracted off its bottom so as to accurately locate the peak positions (shown as red dots). The dash-dotted curve corresponds to an η value of $1.81\eta_0$, with $\eta_0 = \sqrt{\epsilon m}/\sigma^2$, in good agreement with that obtained in the hydrophilic case. Note that bulk viscosity only depends on the fluid-fluid interaction and the two sets of simulations should therefore give the same value for η . (b) For $H = 26.1\sigma$, seven modes can be identified, with their k positions indicated by the red triangles (see Table II). These k 's uniquely determine a value of $h = 23.6\sigma$, or $\Delta = 2.5\sigma$. The consistency in the value of Δ with the case shown in (a) also indicates that it is an interfacial characteristic. From the dash-dotted curve, the η value is estimated to be $1.81\eta_0$. (c) For $H = 51.9\sigma$, the number of discernible modes has now increased to 16 (see Table II). Their agreement with the theory predictions is within 1%. Here $\Delta = 2.2\sigma$. An η value of $1.83\eta_0$ is obtained. The slipping lengths obtained from the three cases are 3.0σ , 3.0σ , and 3.1σ for (a), (b), and (c), respectively. It is noted that, for the present hydrophobic case, l_{slip} has increased by about 50% as compared to the hydrophilic case. It is also noted to be larger than Δ .

only on the fluid-fluid interaction, which remains unchanged. The consistent result for fluid viscosity obtained from all the simulations further reveals the fact that the fluid density is well maintained for all the simulations [41]. However, the slip length exhibits a $\sim 50\%$ increase from the hydrophilic case, to 3σ , while the value of Δ remains about the same. The value of the interfacial dissipation coefficient is obtained to be $\beta = 0.6\sqrt{\epsilon m}/\sigma^3$, much smaller than in the hydrophilic case as expected.

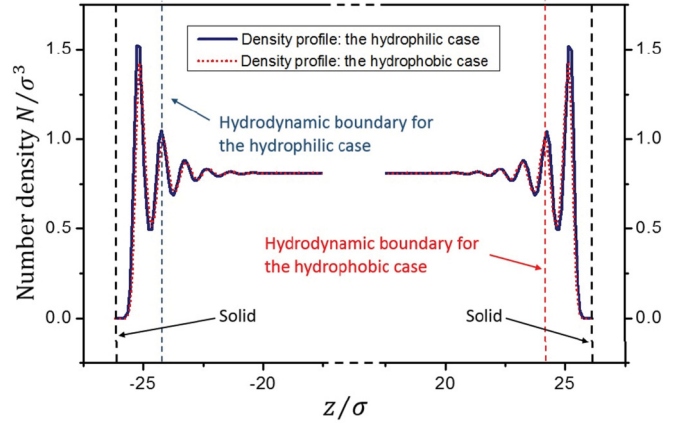


FIG. 7. (Color online) Number density profile across the channel. Here the hydrophobic case is delineated by the dotted red curve, and the hydrophilic case is delineated by the dark blue solid curve. The curves are truncated in order to enlarge the profiles near the solid interface. Convergence of the density to a common value is clearly seen. The positions of the hydrodynamic boundaries are indicated by the black and red dashed lines for the hydrophilic and hydrophobic cases, respectively. There are only very small differences between the hydrophilic and the hydrophobic cases, since the changes in the LJ parameters between the two are small. The vertical dashed black lines indicate the positions of the first layer of solid atoms. The vertical dashed dark blue line and the vertical dashed red line indicate the positions of hydrodynamic boundaries for the hydrophilic and hydrophobic cases, respectively. For each case, only one boundary is marked so as to allow a clear view.

The relatively small change in Δ agrees well with the estimation of $\sim 0.1\sigma$ increment in the equilibrium wall-fluid atomic distance as a result of the adjustment of δ_{wf} from 1 to 0.7 [13]. This fact can be clearly seen from the plot of the fluid number density profile across the $H_2 = 26.1\sigma$ channel for both the hydrophilic (dark blue solid curve) and the hydrophobic (dotted red curve) cases, as shown in Fig. 7. The number density profiles reveal that (1) the fluid atoms form strongly layered structures at the fluid-solid interface for both cases, which is the usual behavior for a wetting fluid; (2) the positions of the density peaks slightly shift away from the wall by $\sim 0.1\sigma$ when δ_{wf} is adjusted from 1 to 0.7, and the heights of the peaks decrease, implying that the fluid is less wetting to the wall for the case of $\delta_{wf} = 0.7$; (3) the bulk density is well maintained in both cases; and (4) the position of the hydrodynamic boundary is near the second-highest peak in the density profile in both cases. It should be noted that there has been a previous report of an interfacial fluid layer, generally a few molecular diameters in thickness, over which the viscosity and diffusion constant differ from their bulk values [29]. This observation is consistent with the density layers and the position of the hydrodynamic boundary described above.

The k_n values measured in MD simulations are tabulated in Table II, and compared with their respective theory predictions. Except for one peak in the large-channel case that cannot be well resolved, all the other peaks exhibit excellent agreement. This consistency gives confidence in the location of the hydrodynamic boundary and the relevant parameter values.

TABLE II. Parameter values for the hydrophobic case.

		$(k_n \text{ in units of } 1/\sigma)$						
		$H = 13.2\sigma, h = 10.8 \pm 0.2\sigma, \Delta = 2.4 \pm 0.2\sigma, l_{\text{slip}} = 3.0 \pm 0.1\sigma, \eta = 1.81\eta_0$						
k_n MD	0.235			0.492				0.767
k_n Theory	0.234			0.492				0.767
		$H = 26.1\sigma, h = 23.6 \pm 0.2\sigma, \Delta = 2.5 \pm 0.2\sigma, l_{\text{slip}} = 3.0 \pm 0.1\sigma, \eta = 1.81\eta_0$						
k_n MD	0.119	0.242	0.367	0.491	0.619	0.744		0.873
k_n Theory	0.119	0.240	0.364	0.492	0.621	0.751		0.882
		$H = 51.9\sigma, h = 49.7 \pm 0.2\sigma, \Delta = 2.2 \pm 0.2\sigma, l_{\text{slip}} = 3.1 \pm 0.1\sigma, \eta = 1.83\eta_0$						
k_n MD	0.0593	0.12	0.179	0.24	0.301	0.365	0.421	0.489
k_n Theory	0.0595	0.119	0.179	0.24	0.301	0.362	0.424	0.486
k_n MD	0.55	0.609	0.677	0.736	0.804	0.866	–	0.983
k_n Theory	0.548	0.610	0.672	0.735	0.798	0.861	0.924	0.986

VI. GREEN-KUBO RELATION FOR A FINITE FLUID SYSTEM

To complete the picture, it is important that we have an overall picture of the FDT for a finite fluid bounded by solid walls, so that the condition for the emergence of an independent interfacial FDT may be clarified. This would better connect the present work with the previous literature.

Consider the system shown in Fig. 8. Here we consider only the domain over which the hydrodynamic description applies, i.e., $z = \pm h$. Hence the “wall” shown in the figure automatically includes the fluid layer denoted by Δ . By removing the center of mass from our considerations, only the antisymmetric fluctuating modes for an incompressible fluid need to be considered. Since we wish to include in our consideration the interfacial dissipation, the system will contain a thin lubrication layer next to the wall, with some artificial viscosity denoted as η_2 that is taken to be proportional to the thickness of the lubrication layer, denoted by l . The bulk viscosity is denoted by η_1 . At the end of the derivation we shall see that $l = l_{\text{slip}}$ if we set $\eta_2 = \eta_1$. We specify the velocity \mathbf{v} (both normal and tangential components) to be zero at the interface between the wall and the boundary layer.

The strategy we wish to pursue is to combine the bulk and interfacial dissipations into a single system for unified treatment. By letting l to approach zero (but maintaining η_2/l to be a constant) and h to approach infinity, we can separate out the interfacial component at the end.

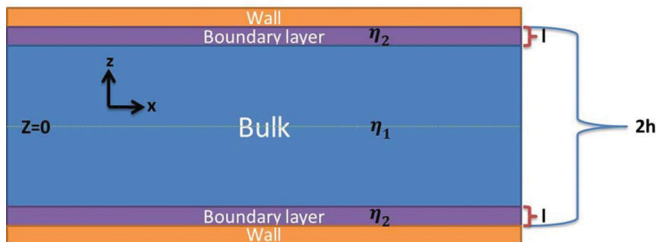


FIG. 8. (Color online) Geometry of the system under consideration. In order to consider the bulk and interfacial dissipations as a single system for unified treatment, the interfacial region is artificially magnified and endowed with an artificial viscosity coefficient η_2 .

The fluctuating transverse momentum (x component) density is defined by $J(z, t) = \rho_0 v(z, t)$. Its eigenvectors $j_n(z, t)$ can be obtained by solving Eqs. (1) and (2). From Eq. (2a), the antisymmetric solutions are given by $Z_n(z) = A_n \sin(k_n z)$ for z within the region of $\pm[0, h - l]$, and $Z_n(z) = V_n^S (h - z)/l$ for z within the region of $\pm[h - l, h]$, valid for $k_n l \ll 1$. Here we have defined the (slip) velocity $v_n^S = V_n^S / \rho_0$ at $z = h - l$. In addition, the condition $Z_n(z = \pm h) = 0$ is noted to be contained in the form of the solution in the lubrication layer region. From Eq. (2b), we obtain $T_n(t) = \exp[-t/(\rho_0/\eta_1 k_n^2)]$ by setting $T_n(0) = 1$.

The solution in the two regions must satisfy the interfacial conditions of tangential stress and transverse momentum density be continuous at $z = h - l$:

$$V_n^S = A_n \sin[k_n(h - l)], \quad (6)$$

$$-\eta_2 V_n^S / l = \eta_1 A_n k_n \cos[k_n(h - l)]. \quad (7)$$

Dividing Eq. (6) by Eq. (7), we obtain the eigenvalue equation

$$\tan[k_n(h - l)] = -\frac{\eta_1 k_n l}{\eta_2}. \quad (8)$$

In the following we wish to (a) apply the equipartition theorem to each of the hydrodynamic modes, and (b) write down the traditional FDT for the whole domain $z = \pm h$ in which we have only viscous dissipation.

A. Application of the equipartition theorem

The application of the equipartition theorem $2S \int_0^h Z_n(z)^2 dz = \rho_0 k_B T$ leads to

$$2S \left[\int_0^{h-l} A_n^2 \sin^2(k_n z) dz + \int_{h-l}^h \left(\frac{V_n^S}{l} (h - z) \right)^2 dz \right] = \rho_0 k_B T. \quad (9)$$

The first and second terms on the left-hand side of Eq. (9) represent the bulk and boundary contributions, respectively, and the factor of 2 is present because we have two halves and hence two interfaces in the present case. Since A_n and V_n^S are

present in both Eqs. (6) and (9), they can be solved to yield

$$A_n^2 = \frac{\rho_0 k_B T}{S \left[h - l - \frac{\sin[2k_n(h-l)]}{2k_n} + \frac{2l \sin^2[k_n(h-l)]}{3} \right]}, \quad (10)$$

$$(V_n^S)^2 = \frac{\sin^2[k_n(h-l)] \rho_0 k_B T}{S \left[h - l - \frac{\sin[2k_n(h-l)]}{2k_n} + \frac{2l \sin^2[k_n(h-l)]}{3} \right]}. \quad (11)$$

From the eigenvalue Eq. (8), we can get

$$\sin[2k_n(h-l)] = \frac{2 \tan[k_n(h-l)]}{1 + \tan^2[k_n(h-l)]} = -\frac{2\eta_1 \eta_2 l k_n}{\eta_2^2 + \eta_1^2 l^2 k_n^2}, \quad (12)$$

$$\sin^2[k_n(h-l)] = \frac{1}{2} \left(1 - \frac{1 - \tan^2[k_n(h-l)]}{1 + \tan^2[k_n(h-l)]} \right) = \frac{\eta_1^2 l^2 k_n^2}{\eta_2^2 + \eta_1^2 l^2 k_n^2}. \quad (13)$$

Application of the FDT for viscous dissipation

The FDT for each mode of the whole system may now be written as

$$2S \int_0^{+\infty} dt \int_0^h dz \left(\eta \left\langle \left(\frac{\partial j_n(z,t=0)}{\partial z} \right) \left(\frac{\partial j_n(z,t)}{\partial z} \right) \right\rangle \right) = \rho_0^2 k_B T, \quad (14)$$

where the angular brackets denote statistical thermal averaging, the effect of which is essentially the equipartition condition that we have expressed above already, and $\eta = \eta_1$ for z in the region of $\pm[0, h-l]$, and $\eta = \eta_2$ for z in the region of $\pm[h-l, h]$. Equation (14) can be expressed as

$$2S \left[\int_0^h \eta_1 \left(\frac{\partial Z_n(z)}{\partial z} \right)^2 dz + \beta (V_n^S)^2 \right] \int_0^{+\infty} T_n(t) dt = \rho_0^2 k_B T, \quad (15)$$

where $\beta = \eta_2/l$. The bulk and boundary layer dissipation components can be clearly seen as the two terms in the square brackets. In fact, it is straightforward to show that if $V_n^S = 0$, i.e., for the nonslip case, then Eq. (15) is an identity, $\eta_1 = \eta_1$.

To proceed further, we wish to evaluate the boundary layer and the bulk dissipations, D_n^{boundary} and D_n^{bulk} , in the limit of $h/l \gg 1$. With the aid of Eqs. (12) and (13), we obtain

$$D_n^{\text{boundary}} = 2S\beta (V_n^S)^2 \rightarrow \frac{\eta_1 k_n^2 \rho_0 k_B T}{1 + \frac{\eta_1 \beta}{h(\beta^2 + \eta_1^2 k_n^2)}} \frac{2\eta_1 \beta}{h(\beta^2 + \eta_1^2 k_n^2)} \quad (16)$$

and

$$D_n^{\text{bulk}} = S\eta_1 A_n^2 k_n^2 \left(h - l + \frac{\sin[2k_n(h-l)]}{2k_n} \right) \rightarrow \frac{\eta_1 k_n^2 \rho_0 k_B T}{1 + \frac{\eta_1 \beta}{h(\beta^2 + \eta_1^2 k_n^2)}} \times \left(1 - \frac{\eta_1 \beta}{h(\beta^2 + \eta_1^2 k_n^2)} \right). \quad (17)$$

B. Defining the fraction of boundary dissipation

One can define a dimensionless boundary dissipation fraction C_n for each mode:

$$C_n = \frac{1}{2} \frac{D_n^{\text{boundary}}}{D_n^{\text{bulk}} + D_n^{\text{boundary}}} = \frac{\eta_1 \beta}{h(\beta^2 + \eta_1^2 k_n^2) + \eta_1 \beta}. \quad (18)$$

The FDT for the boundary momentum density fluctuation for one mode, in the large h/l limit, can now be written as

$$S\beta (V_n^S)^2 \int_0^{+\infty} T_n(t) dt \cong C_n \rho_0^2 k_B T,$$

or more generally as

$$\int_0^{+\infty} \langle j_n(z=h, t=0) j_n(z=h, t) \rangle dt \cong \frac{C_n \rho_0^2 k_B T}{S\beta}. \quad (19)$$

From Eq. (14), the total bulk and boundary dissipation in the large h/l limit may be expressed as

$$\begin{aligned} 2S \sum_{n=0}^{\infty} \left[\int_0^h \eta_1 \left(\frac{\partial Z_n(z)}{\partial z} \right)^2 dz + \beta (V_n^S)^2 \int_0^{+\infty} T_n(t) dt \right] \\ = 2S \int_0^{+\infty} dt \int_0^h dz \left\langle \eta_1 \left(\frac{\partial J(z, t=0)}{\partial z} \right) \left(\frac{\partial J(z, t)}{\partial z} \right) \right\rangle \\ + 2S\beta \int_0^{+\infty} dt \langle J(z=h, t=0) J(z=h, t) \rangle \\ \cong \sum_{n=0}^{\infty} (1 - 2C_n) \rho_0^2 k_B T + \sum_{n=0}^{\infty} 2C_n \rho_0^2 k_B T. \end{aligned} \quad (20)$$

In the above, C_n is noted to be a function of h/l , and we have used the relation

$$\begin{aligned} \langle J(z=h, t=0) J(z=h, t) \rangle \\ = \sum_{n=0}^{\infty} j_n(z=h, t=0) j_n(z=h, t) = \sum_{n=0}^{\infty} (V_n^S)^2 T_n(t). \end{aligned}$$

C. Separate FDTs for bulk and interfacial dissipations

The bulk FDT can now be written as

$$\begin{aligned} \int_0^{+\infty} dt \int_0^h dz \left\langle \left(\frac{\partial J(z, t=0)}{\partial z} \right) \left(\frac{\partial J(z, t)}{\partial z} \right) \right\rangle \\ = \frac{\rho_0^2 k_B T}{2S\eta_1} \sum_{n=0}^{\infty} (1 - 2C_n), \end{aligned} \quad (21)$$

whereas the boundary FDT is given by

$$\int_0^{+\infty} \langle J(z=h, t=0) J(z=h, t) \rangle dt = \frac{\rho_0^2 k_B T}{S\beta} \sum_{n=0}^{\infty} C_n. \quad (22)$$

We have numerically evaluated the sum $\sum_{n=0}^{\infty} C_n = \Xi$, which is shown in Fig. 9 as a function of h/l . It is seen that $\Xi \rightarrow 1/2$ as $h/l \rightarrow \infty$. Hence in the limit of $h/l \rightarrow \infty$ the bulk dissipation is proportional to $N - 1$, where the total number of modes $N \rightarrow \infty$. The boundary FDT, on the other hand, displays an h -dependent form, which (except for a factor of 2 since here we have two interfaces) is exactly the expression given by Bocquet and Barrat [9] in the limit of $h/l \rightarrow \infty$. In practical terms, Bocquet and Barrat's expression

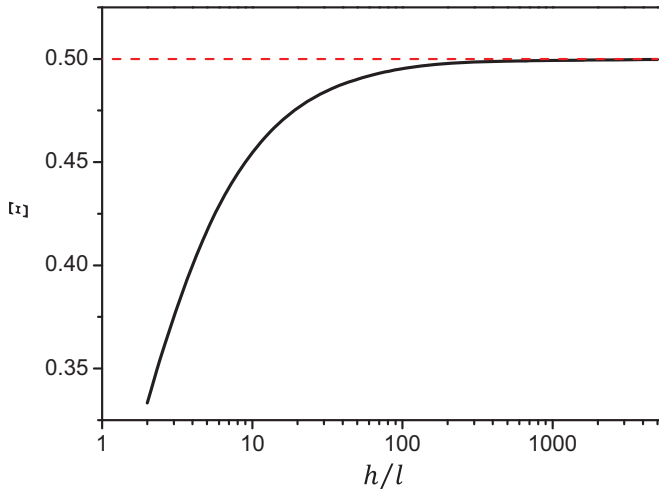


FIG. 9. (Color online) The h dependence of Ξ . The asymptotic approach to the limiting value, shown as the red dashed line, has the form $\Xi \cong 1/2 - l/2h$ as $h/l \rightarrow \infty$.

could be close to being valid when h is at least two orders of magnitude larger than l , since Ξ is nearly sample-size independent in that regime.

The lesson learned from this derivation is that, for small h/l , the boundary and bulk dissipations are inseparable, and the finite-size simulation of the boundary FDT would lead to a clear size dependence as observed previously [12,13,21]. Separation of the two components, with size independence of the boundary FDT, is achieved only at the large h/l limit.

VII. CONCLUDING REMARKS

By using molecular dynamics to evaluate the time correlation function of projected hydrodynamic modes, we have generalized the FDT to the case of a finite fluid system bounded by solid walls. From the multiple-peak structure of the k spectrum of the decay time, we are able to relate the information obtained from microscopic equilibrium fluctuations to the parameters of the macroscopic hydrodynamic boundary condition. By showing that such information is inherently contained in fluctuating modes, the present approach has opened up obvious but nontrivial extensions to cases involving chemically patterned or geometrically undulating interfaces, soft elastic boundaries, and two-phase immiscible fluids separated by a contact line at the solid wall. Application of the present approach to the latter may yield parameters of the moving contact line boundary condition [22–24,33] that can shed further light on this classical problem.

ACKNOWLEDGMENTS

P.S. wishes to acknowledge the support of SRFI11/SC02, William Mong Institute of Nanoscience and Technology Grant No. R1X21, and Research Grants Council Grant No. HKUST603512. T.Q. wishes to acknowledge the support of Research Grants Council Grant No. HKUST604013. H.W. wishes to acknowledge the support of National High Technology Research and Development Program of China Grant No. 2015AA011201.

S.C. and H.W. contributed equally to this work.

-
- [1] J. C. Maxwell, On the dynamical theory of gases, *Philos. Trans. R. Soc. London* **157**, 49 (1867).
 - [2] J. C. Maxwell, On stresses in rarified gases arising from inequalities of temperature, *Philos. Trans. R. Soc. London Ser. A* **170**, 231 (1879).
 - [3] S. Chen and G. D. Doolen, Lattice Boltzmann method for fluid flows, *Annu. Rev. Fluid Mech.* **30**, 329 (1998).
 - [4] S. Shen, G. Chen, R. M. Crone, and M. Anaya-Dufresne, A kinetic-theory based first order slip boundary condition for gas flow, *Phys. Fluids* **19**, 086101 (2007).
 - [5] C. K. Aidun and J. R. Clausen, Lattice-Boltzmann method for complex flows, *Annu. Rev. Fluid Mech.* **42**, 439 (2010).
 - [6] F. C. Wang and Y. P. Zhao, Slip boundary conditions based on molecular kinetic theory: The critical shear stress and the energy dissipation at the liquid–solid interfac, *Soft Matter* **7**, 8628 (2011).
 - [7] Z. Guo, J. Qin, and C. Zheng, Generalized second-order slip boundary condition for nonequilibrium gas flows, *Phys. Rev. E* **89**, 013021 (2014).
 - [8] P. G. Wolynes, Hydrodynamic boundary conditions and mode-mode coupling theory, *Phys. Rev. A* **13**, 1235 (1976).
 - [9] L. Bocquet and J. L. Barrat, Hydrodynamic boundary conditions, correlation functions, and Kubo relations for confined fluids, *Phys. Rev. E* **49**, 3079 (1994).
 - [10] J. Petracic and P. Harrowell, The boundary fluctuation theory of transport coefficients in the linear-response limit, *J. Chem. Phys.* **124**, 014103 (2006).
 - [11] L. Bocquet and J. L. Barrat, Flow boundary conditions from nano- to micro-scales, *Soft Matter* **3**, 685 (2007).
 - [12] J. Petracic and P. Harrowell, On the equilibrium calculation of the friction coefficient for liquid slip against a wall, *J. Chem. Phys.* **127**, 174706 (2007).
 - [13] J. Petracic and P. Harrowell, Equilibrium calculations of viscosity and thermal conductivity across a solid-liquid interface using boundary fluctuations, *J. Chem. Phys.* **128**, 194710 (2008).
 - [14] A. E. Kobryn and A. Kovalenko, Molecular theory of hydrodynamic boundary conditions in nanofluidics, *J. Chem. Phys.* **129**, 134701 (2008).
 - [15] L. Bocquet and E. Charlaix, Nanofluidics, from bulk to interfaces, *Chem. Soc. Rev.* **39**, 1073 (2010).
 - [16] J. S. Hansen, B. D. Todd, and P. J. Daivis, Prediction of fluid velocity slip at solid surfaces, *Phys. Rev. E* **84**, 016313 (2011).
 - [17] F. Detcheverry and L. Bocquet, Thermal Fluctuations in Nanofluidic Transport, *Phys. Rev. Lett.* **109**, 024501 (2012).
 - [18] S. K. Kannam, B. D. Todd, J. S. Hansen, and P. J. Daivis, Interfacial slip friction at a fluid-solid cylindrical boundary, *J. Chem. Phys.* **136**, 244704 (2012).
 - [19] F. Detcheverry and L. Bocquet, Thermal fluctuations of hydrodynamic flows in nanochannels, *Phys. Rev. E* **88**, 012106 (2013).
 - [20] L. Bocquet and J. L. Barrat, On the Green-Kubo relationship for the liquid-solid friction coefficient, *J. Chem. Phys.* **139**, 044704 (2013).
 - [21] K. Huang and I. Szlufarska, Green-Kubo relation for friction at liquid-solid interfaces, *Phys. Rev. E* **89**, 032119 (2014).

- [22] T. Qian, X. P. Wang, and P. Sheng, Molecular scale contact line hydrodynamics of immiscible flows, *Phys. Rev. E* **68**, 016306 (2003).
- [23] T. Qian, X. P. Wang, and P. Sheng, Power-Law Slip Profile of the Moving Contact Line in Two-Phase Immiscible Flows, *Phys. Rev. Lett.* **93**, 094501 (2004).
- [24] T. Qian, X. P. Wang, and P. Sheng, A variational approach to moving contact line hydrodynamics, *J. Fluid Mech.* **564**, 333 (2006).
- [25] P. A. Thompson and S. M. Troian, A general boundary condition for liquid flow at solid surfaces, *Nature* **389**, 360 (1997).
- [26] J. L. Barrat and L. Bocquet, Large Slip Effect at a Nonwetting Fluid-Solid Interface, *Phys. Rev. Lett.* **82**, 4671 (1999).
- [27] M. Cieplak, J. Koplik, and J. R. Banavar, Boundary Conditions at a Fluid-Solid Interface, *Phys. Rev. Lett.* **86**, 803 (2001).
- [28] N. V. Priezjev, Rate-dependent slip boundary conditions for simple fluids, *Phys. Rev. E* **75**, 051605 (2007).
- [29] C. Denniston and M. O. Robbins, General continuum boundary conditions for miscible binary fluids from molecular dynamics simulations, *J. Chem. Phys.* **125**, 214102 (2006).
- [30] V. S. J. Craig, C. Neto, and D. R. M. Williams, Shear-Dependent Boundary Slip in an Aqueous Newtonian Liquid, *Phys. Rev. Lett.* **87**, 054504 (2001).
- [31] P. Joseph and P. Tabeling, Direct measurement of the apparent slip length, *Phys. Rev. E*, **71**, 035303 (2005).
- [32] J. P. Rothstein, Slip on superhydrophobic surfaces. *Annu. Rev. Fluid Mech.* **42**, 89 (2010).
- [33] S. Guo, M. Gao, X. Xiong, Y. J. Wang, X. Wang, P. Sheng, and P. Tong, Direct Measurement of Friction of a Fluctuating Contact Line, *Phys. Rev. Lett.* **111**, 026101 (2013).
- [34] R. Kubo, The fluctuation-dissipation theorem, *Rep. Prog. Phys.* **29**, 255 (1966).
- [35] M. S. Green, Markoff random processes and the statistical mechanics of time-dependent phenomena. II. Irreversible processes in fluids, *J. Chem. Phys.* **22**, 398 (1954).
- [36] R. Kubo, Statistical-mechanical theory of irreversible processes. I. General theory and simple applications to magnetic and conduction problems, *J. Phys. Soc. Jpn.* **12**, 570 (1957).
- [37] M. Tuckerman, *Statistical Mechanics: Theory and Molecular Simulation* (Oxford University Press, Oxford, 2010).
- [38] P. A. Thompson and M. O. Robbins, Shear flow near solids: Epitaxial order and flow boundary conditions, *Phys. Rev. A* **41**, 6830 (1990).
- [39] D. Frenkel and B. Smit, *Understanding Molecular Simulation from Algorithms to Applications*, 2nd ed. (Academic Press, San Diego, 2002).
- [40] D. M. Heyes, Shear thinning and thickening of the Lennard-Jones liquid. A molecular dynamics study, *J. Chem. Soc., Faraday Trans. 2* **82**, 1365 (1986).
- [41] K. Meier, A. Laesecke, and S. Kabelac, Transport coefficients of the Lennard-Jones model fluid. I. Viscosity, *J. Chem. Phys.* **121**, 3671 (2004).